nature astronomy

LETTERS

https://doi.org/10.1038/s41550-020-1066-7

Check for updates

An extremely energetic supernova from a very massive star in a dense medium

Matt Nicholl[1,2,3]✉, Peter K. Blanchard[4,5,6], Edo Berger[6], Ryan Chornock[7], Raffaella Margutti[4,5], Sebastian Gomez[6], Ragnhild Lunnan[8,9], Adam A. Miller[4,5,10], Wen-fai Fong[4,5], Giacomo Terreran[4,5], Alejandro Vigna-Gómez[11], Kornpob Bhirombhakdi[12], Allyson Bieryla[6], Pete Challis[6], Russ R. Laher[13], Frank J. Masci[13] and Kerry Paterson[4,5]

The interaction of a supernova with a circumstellar medium (CSM) can dramatically increase the emitted luminosity by converting kinetic energy to thermal energy. In 'superluminous' supernovae of type IIn—named for narrow hydrogen lines[1] in their spectra—the integrated emission can reach[2–6] ~10^{51} erg, attainable by thermalizing most of the kinetic energy of a conventional supernova. A few transients in the centres of active galaxies have shown similar spectra and even larger energies[7,8], but are difficult to distinguish from accretion onto the supermassive black hole. Here we present a new event, SN2016aps, offset from the centre of a low-mass galaxy, that radiated $\gtrsim 5\times10^{51}$ erg, necessitating a hyper-energetic supernova explosion. We find a total (supernova ejecta + CSM) mass likely exceeding 50–100 $M_\odot$, with energy $\gtrsim10^{52}$ erg, consistent with some models of pair-instability supernovae or pulsational pair-instability supernovae—theoretically predicted thermonuclear explosions from helium cores >50 $M_\odot$. Independent of the explosion mechanism, this event demonstrates the existence of extremely energetic stellar explosions, detectable at very high redshifts, and provides insight into dense CSM formation in the most massive stars.

SN2016aps (internal designation, PS16aqy) was discovered by the Panoramic Survey Telescope and Rapid Response System (Pan-STARRS) Survey for Transients[9] on 22 February 2016 UT with an apparent magnitude $m = 18.12 \pm 0.08$ mag in the i-band (7,545 Å). We selected this target for spectroscopic follow-up due to its large brightness contrast relative to the previously undetected host galaxy, with $m \gtrsim 23.5$ mag in Pan-STARRS1 3π survey data. Our first spectrum[10], on 2 March 2016 UT, showed hydrogen Balmer emission lines at a redshift of $z = 0.2657$, and hence an absolute magnitude of $M = -22.5 \pm 0.08$ mag at the time of discovery (Methods). A search of archival images from the intermediate Palomar Transient Factory[11] revealed a rising light curve going back to at least 2 December 2015 UT, with maximum brightness on 17 January 2016 UT. We obtained further spectra spanning 500 d, and optical and ultraviolet (UV) imaging spanning 1,000 d. All phases are in the supernova (SN) rest frame relative to the date of maximum brightness.

We imaged the location of SN2016aps 1,017 rest-frame days after maximum brightness using the Hubble Space Telescope (HST), identifying the previously undetected host galaxy (Fig. 1). The absolute magnitude of the galaxy in the HST F775W filter, $M_{\rm F775W} = -17$ mag (intermediate between the Small and Large Magellanic Clouds), indicates a stellar mass $M_* \approx 10^8 M_\odot$ (assuming $M_*/M_\odot \approx L_*/L_\odot$, where L_* is the stellar luminosity) and likely a subsolar metallicity (Methods). A compact bright region, visible in both the F775W-band (optical) and F390W-band (UV) images, is coincident with the SN position and significantly offset from the centre of the galaxy by $0.15'' \pm 0.03''$ (Methods). While some energetic, often hydrogen-rich transients may represent supermassive

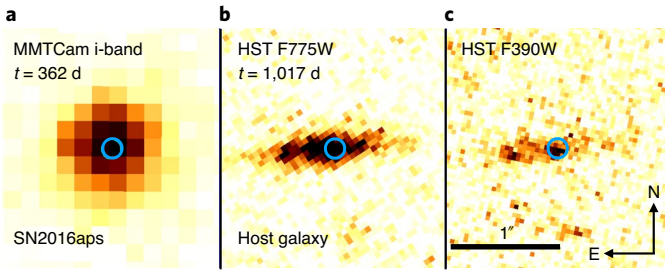

Fig. 1 | Ground-based and HST images of SN2016aps and its host galaxy. **a**, MMTCam i-band (7,730 Å) image of SN2016aps at a phase of 362 d. **b**, HST optical F775W-band image of the host galaxy obtained at a phase of 1,017 d. **c**, HST UV F390W-band image of the host galaxy at the same phase. All images were astrometically aligned using a catalogue of matched sources in the field of view (not shown at this scale). The blue circle shows the position of SN2016aps, as measured in the MMTCam image, with its radius equal to the combined 3σ error from determining the centroid and aligning the MMT image to the HST images (Methods). SN2016aps is coincident with the brightest UV-emitting region of its host galaxy, providing a direct connection with ongoing star-formation activity. The location of SN2016aps is 0.15″ from the optical centre of its host galaxy.

[1]Birmingham Institute for Gravitational Wave Astronomy, University of Birmingham, Birmingham, UK. [2]School of Physics and Astronomy, University of Birmingham, Birmingham, UK. [3]Institute for Astronomy, University of Edinburgh, Royal Observatory, Blackford Hill, UK. [4]Department of Physics and Astronomy, Northwestern University, Evanston, IL, USA. [5]Center for Interdisciplinary Exploration and Research in Astrophysics (CIERA), Northwestern University, Evanston, IL, USA. [6]Center for Astrophysics | Harvard & Smithsonian, Cambridge, MA, USA. [7]Astrophysical Institute, Department of Physics and Astronomy, Ohio University, Athens, OH, USA. [8]Oskar Klein Centre, Department of Astronomy, Stockholm University, Stockholm, Sweden. [9]The Adler Planetarium, Chicago, IL, USA. [10]Department of Astronomy, California Institute of Technology, Pasadena, CA, USA. [11]DARK, Niels Bohr Institute, University of Copenhagen, Copenhagen, Denmark. [12]Space Telescope Science Institute, Baltimore, MD, USA. [13]IPAC, California Institute of Technology, Pasadena, CA, USA. ✉e-mail: mnicholl@star.sr.bham.ac.uk

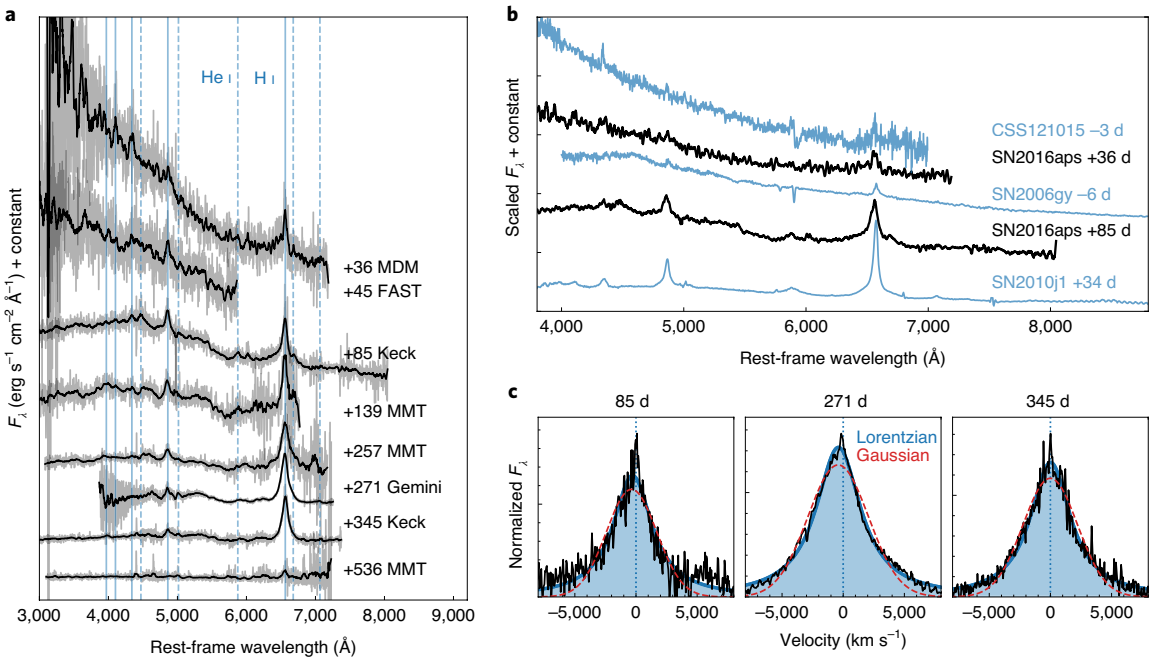

Fig. 2 | Spectroscopic evolution of SN2016aps over 500 rest-frame days following discovery. a, The spectra (in flux density per unit wavelength, F_λ) have been smoothed using a Savitsky–Golay filter, with lighter colours showing the original unsmoothed data, and offset for clarity. Phases (days since maximum brightness) are labelled in the SN rest frame, based on a redshift of $z = 0.2657$. Vertical lines mark the dominant emission lines from neutral hydrogen and helium. **b**, Comparison of two representative spectra of SN2016aps to other[2,6,14] SLSNe IIn. SN2016aps shows an early blue continuum and Balmer lines that increase in equivalent width over time, similar to previous events. **c**, Continuum-subtracted Hα emission in the high signal-to-noise ratio spectra from Gemini and Keck. Gaussian and Lorentzian functions have been fitted to the line profiles, with the latter better reproducing the narrow core and broad wings. The velocity full-width at half-maximum is $4{,}090 \pm 230$ km s^{-1} (1σ) at 80–350 d, indicating[14] an optical depth $\tau \gtrsim 6$ to Hα photons.

black hole accretion rather than supernovae (SNe)[7,8,12], the faint galaxy and offset from the nucleus require a SN origin for SN2016aps. The UV image shows that it occurred in the brightest star-forming region within the galaxy, pointing to a massive star progenitor.

The spectra (Fig. 2) are typical of 'superluminous' supernovae (SLSNe) of type IIn[2,6], while the peak absolute magnitude is equal to the most luminous[6] events (Fig. 3). What sets SN2016aps apart from all previous events is the unprecedented combination of a large peak luminosity characteristic of the brightest 'compact shell'[2] SLSNe IIn and a slow rate of fading (0.8 mag per 100 d), similar to long-lived events[13,14], thought to have more extended circumstellar medium (CSM). To measure the total optical output of SN2016aps, we integrate our photometry at each point in the light curve, and fit a blackbody function to estimate the flux outside of the observed bands (Methods). The radius is roughly constant at 5×10^{15} cm, while the temperature decreases from 10,000 K near peak to 6,000 K after 200 d (Extended Data Fig. 1). The peak luminosity is 4.3×10^{44} erg s^{-1}, and the integrated energy radiated over the time of our observations is $E_{\rm rad} = (5.0 \pm 0.1) \times 10^{51}$ erg. This is the largest radiated energy for any confirmed SN; the maximum observed energy for previous SLSNe is[2–6] ~2×10^{51} erg. It was argued[5] that SN2003ma may have emitted up to 4×10^{51} erg, but this is highly uncertain as only 20% of this energy was within the wavelength range covered by observations, compared with 70% for SN2016aps. Where a normal SN has (just) enough kinetic energy to power previous SLSNe IIn, the total emission from SN2016aps cannot be explained without a hyperenergetic explosion[15].

Assuming the light curve is powered by shock heating of CSM, we use common relations[16] to estimate the kinetic energy and shock velocity from the luminosity and total emission (Supplementary Information). We find an explosion energy $E_{\rm K}^2/M_{\rm ej} = 4.9$ (in units of 10^{51} erg and $M_\odot$) and a shock velocity of $v_{\rm s} \approx 4{,}600$ km s^{-1}. In this model[16], $E_{\rm rad}/E_{\rm K} = 0.32$, giving an ejected mass $M_{\rm ej} \gtrsim 52\,M_\odot$ for our measured $E_{\rm rad} = 5 \times 10^{51}$ erg. We map the pre-explosion mass loss, $\dot{M}$, by inverting the bolometric light curve according to[17] $L = \frac{1}{2}\psi \dot{M} v_{\rm s}^3 / v_{\rm w}$, where $v_{\rm s}$ is the shock velocity and $\psi \approx 0.5$ is the efficiency[18] of converting kinetic energy to radiation. This gives $\dot{M} \approx 0.1$–$10\,M_\odot$ yr^{-1} for a wind with velocity $v_{\rm w} = 10$–$1{,}000$ km s^{-1} (Fig. 4). We can estimate the time of mass ejection as $R_{\rm s}/v_{\rm w}$, where the shock radius $R_{\rm s} = v_{\rm s}(t - t_{\rm explosion})$ at time t. The integrated CSM mass, lost years to centuries before explosion, is $M_{\rm CSM} \gtrsim 40\,M_\odot$. Photoionization from external UV radiation in the local star-forming region may help to confine this mass loss close to the progenitor[19]. However, compared with a blue supergiant star with $v_{\rm w} \approx 1{,}000$ km s^{-1}, the inferred mass-loss rate exceeds typical[20] values by six orders of magnitude.

As the CSM must be ejected shortly before explosion, a constant density corresponding to a single massive outburst may be more appropriate than a wind. We use the CSM model[21,22] in the Modular Open Source Fitter for Transients (MOSFIT) light-curve fitting package to fit the multiband data (Supplementary Information). Although we can reasonably reproduce the light curve with the parameters estimated above, it underestimates the UV luminosity (Extended Data Fig. 2). If we vary these parameters in a Markov chain Monte Carlo fit, we find that the formal best fit (Fig. 4) has $M_{\rm ej} = 182^{+42}_{-23}\,M_\odot$, $v_{\rm ej} = 6{,}015^{+134}_{-134}$ km s^{-1} and $M_{\rm CSM} = 158^{+23}_{-20}\,M_\odot$ (uncertainties correspond to 1σ range). These posteriors are relatively insensitive to the CSM density profile (Extended Data Figs. 2 and 3). The estimated masses should be treated with caution due to various simplifications (central heat input, constant opacity, neglecting recombination) inherent in modelling a complex process with an analytic formalism. However, the requirement for $\gtrsim$few $\times 10\,M_\odot$ of ejecta and CSM is robust, as evidenced by the long timescale of the light curve and optically thick spectrum, and comparison to

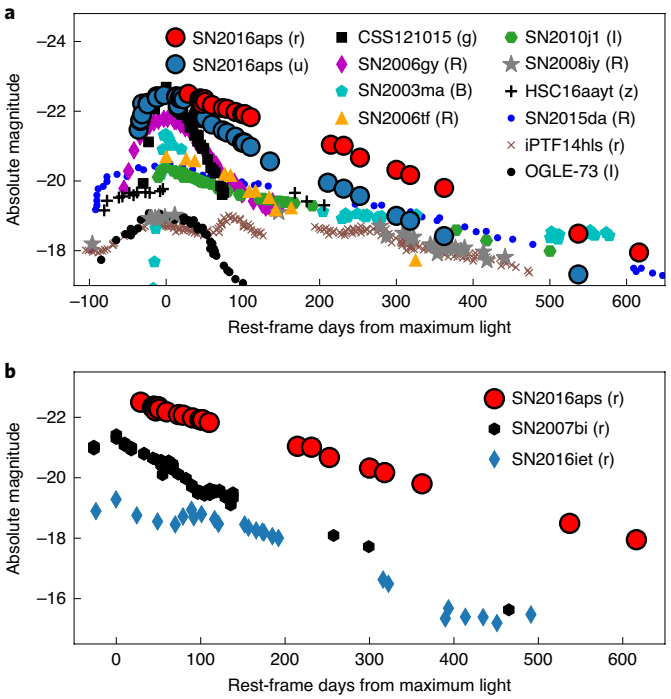

Fig. 3 | Optical light curve of SN2016aps, compared with previous energetic SNe. a, Light curve of SN2016aps in rest-frame r-band (6,260 Å) and u-band (3,560 Å) compared with other luminous and/or long-lived SNe II/IIn on an absolute magnitude scale (Methods). The available band closest to rest-frame r-band was chosen for each comparison SN and is given in brackets in the legend. SN2016aps has a peak brightness at least as bright as any other SLSN IIn, but a slow decline rate (0.78 mag per 100 d in rest-frame r-band) previously only seen in lower-luminosity events, resulting in an integrated electromagnetic output several times greater. **b**, Comparison of SN2016aps to PISN and PPISN candidates, SN2007bi[81] and SN2016iet[25]. SN2016aps clearly exceeds both the peak luminosity and radiated energy of these previous events.

more detailed hydrodynamic models[23] (Fig. 4). We now turn to progenitor and explosion scenarios that can explain the extreme radiated energy in combination with a massive and hydrogen-rich CSM.

Stars with initial masses of 70–140 $M_\odot$ experience large pulsational pair-instability supernova (PPISN) eruptions following core carbon burning[24], before an eventual iron-core collapse. A recent example may have been observed in the hydrogen-poor SN2016iet[25]. Specifically, a progenitor with a helium core ~40–50 $M_\odot$ (total initial mass ~100 $M_\odot$ at the metallicity of the Small Magellanic Cloud) begins pulsing and ejects its envelope a few years before core collapse. Single star models have difficulty retaining hydrogen-rich material until the final years before explosion, but mergers in massive binaries can produce the same core mass while retaining a hydrogen envelope[26]. The rate of mergers in the necessary mass range is estimated[26] to be ~1.4×10^{-3} of the core-collapse SN rate (Methods).

However, the final supernova following the pulses can only meet the observed energy budget of SN2016aps if it forms a millisecond magnetar[24], which then accelerates the ejecta as it spins down. The massive pre-explosion core may require very rapid rotation to avoid collapse to a black hole, but a merger in a binary could conceivably spin up the star to facilitate this process. A millisecond magnetar could also directly contribute to (or even dominate) the radiative output through its spin-down luminosity, relaxing the requirement for a very massive ejecta, but the observed spectrum still requires massive CSM ejected shortly before explosion. Several hydrogen-poor SLSNe[27–29] have shown evidence of CSM shells at larger radii, indicating that engine formation is still possible following mass ejection. The need for a magnetar lowers the predicted rate of SN2016aps-like events, likely by an order of magnitude (Methods). The implied rate of ~10^{-4} per core-collapse SN and ~10^{-1} per SLSN IIn is roughly consistent with not having detected such an event until now.

An exciting alternative is a 'full' pair-instability supernova (PISN) interacting with a dense environment (a non-interacting PISN, even from a very massive star, cannot reach the observed luminosity[15]). Blue supergiant progenitors with zero-age main sequence masses 150–175 $M_\odot$ can retain sufficiently massive helium cores (64–84 $M_\odot$) to encounter a terminal PISN explosion on their second pulse, following an initial failed PISN that expels only the hydrogen envelope[30,31] (a more massive analogue of PPISNe). The kinetic energy of ~10^{52} erg can power an extremely bright interaction. To retain a hydrogen envelope until explosion likely requires a merger in this case too, but avoiding excessive wind losses from the very massive post-merger remnant may necessitate merging only after core helium burning. With such fine-tuning, the predicted rate[26] in this case is ~2×10^{-5} of the core-collapse rate.

Detailed simulations will confirm whether SN2016aps is a PPISN, or even the less likely case of an interacting PISN. This event opens up new possibilities for finding very massive explosions at high redshift, being much brighter than either non-interacting PISNe or PPISNe without a central engine. The brightest radioactively powered PISNe, from 130 $M_\odot$ helium cores, are faint at rest-frame UV wavelengths due to iron group absorption[30]. The Vera C. Rubin Observatory Legacy Survey of Space and Time (LSST) will be able to detect a radioactive PISN at $z\lesssim0.75$, whereas a SN2016aps-like event could be detected out to redshift $z\gtrsim2$ (Methods and Extended Data Fig. 4). This increases the volume over which these massive stars can be detected by a factor of about seven. The PISN candidate[32] SN2213-1745 at redshift $z=2.05$ may have been an analogue of SN2016aps, but was not observed spectroscopically. The upcoming James Webb Space Telescope (JWST) could spectroscopically classify a SN2016aps-like event at $z\gtrsim5$, offering a means to directly probe the deaths of first-generation stars.

Methods

Spectroscopy. We observed SN2016aps spectroscopically using the Ohio State Multi-Object Spectrograph (OSMOS)[33] on the 2.4 m Hiltner telescope at the MDM Observatory, the FAST spectrograph on the Fred Lawrence Whipple Observatory (FLWO) 1.5 m telescope[34], the Blue Channel spectrograph on the MMT[35], the Gemini Multi-Object Spectrograph (GMOS)[36] on Gemini North, and the Low Resolution Imaging Spectrograph (LRIS)[37] on the Keck I 10 m telescope. The majority of these data were reduced in PYRAF (v2.1), applying bias subtraction, flat-fielding and extraction of the one-dimensional spectrum. Wavelength solutions were derived using arc lamps, and flux calibration achieved using observations of standard stars. Keck spectra were reduced using the dedicated LPIPE package[38]. We corrected all spectra for a foreground extinction of $E(B-V)=0.0263$ (ref. [39]) and for a cosmological redshift $z=0.2657$. We assumed a Planck cosmology in all distance calculations[40].

Fits to the line profiles with Gaussian and Lorentzian functions were conducted using SCIPY (v1.3). We approximated the local continuum by fitting a linear function to the following relatively line-free regions. For Hα, we used 6,100–6300 Å and 6,700–6,800 Å and for Hβ we used 4,600–4,780 Å and 4,980–5,000 Å. The profiles are well fit with a Lorentzian function, indicating that broadening is due to electron scattering rather than expansion. Fluxes and equivalent widths were obtained by direct integration. The flux ratio between the Hα and Hβ lines evolves from 2–3 during the first 50 d, to ≳7–10 after 200 d (Extended Data Fig. 5). The early ratio is consistent with hydrogen recombination in ionized CSM, while the late emission can be excited[41] by the passage of shock fronts through the CSM and ejecta. SN2006gy initially exhibited a similar evolution, with an early ratio of ~3, but at times ≳100 d, the ratio increased to more extreme values ~100. However, a direct comparison of these values with SN2016aps may be misleading, as SN2006gy showed substantial absorption components (both narrow and broad) in both emission lines.

The spectra shown in Fig. 2 have been smoothed using a Savitsky–Golay filter[42]. They are initially dominated by a blue continuum superposed with hydrogen Balmer emission lines, typical[2,6] of these events. As the spectra evolve, SN2016aps most closely resembles[13,14] long-duration SLSNe IIn such as SN2010jl and SN2006tf.

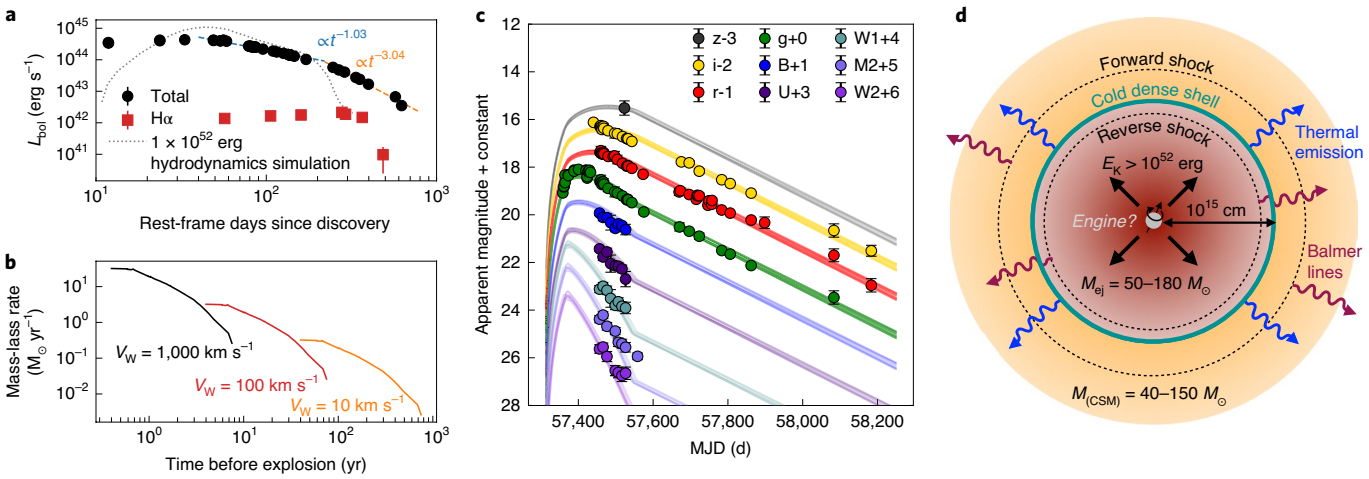

Fig. 4 | Full light curves of SN2016aps and derived properties. a, Bolometric light curve and Hα luminosity. The data can be fitted with a broken power law transitioning from a shallow to a steep decline; the Hα luminosity drops steeply ~100 d later. These drops may indicate the end of shock heating and a transition to diffusion-dominated luminosity[14,41]. Overplotted is a SLSN IIn radiation hydrodynamics model[23] for a CSM mass of 17.3 $M_\odot$ and explosion energy of 10^{52} erg. Although it can reproduce the peak luminosity, a larger mass is needed to match the long timescale of SN2016aps. Error bars show 1σ uncertainties. **b**, Mass-loss history inferred from the bolometric light curve for different assumed wind velocities[17]. The progenitor of SN2016aps requires a mass-loss rate up to six orders of magnitude greater than expected for blue supergiant winds[20]. **c**, Multicolour light curves in optical and UV bands. The legend gives the name of each band and an offset added to the data for clarity of presentation. Error bars show 1σ uncertainties. We overlay realizations of a CSM interaction model[21] from MOSFIT[22]; the best fit has $M_{ej} \approx M_{CSM} \gtrsim 150\,M_\odot$, and $E_K \approx 3 \times 10^{52}$ erg. Acceptable fits are possible with $M_{ej} \gtrsim 50\,M_\odot$, $M_{CSM} \gtrsim 40\,M_\odot$, though these under-predict the UV bands (Methods). **d**, Schematic illustrating the model and inferred parameters. For ejecta (core) masses <65 $M_\odot$ (below the PISN threshold), a magnetar engine may be needed to increase the kinetic energy or luminosity.

SLSNe IIn also share some spectroscopic similarities with energetic nuclear transients[7,8]; however, we argue in the Supplementary Information that these are physically distinct classes. We show a spectroscopic comparison in Extended Data Fig. 6, highlighting notable differences in the Balmer profiles and iron lines.

Photometry. Optical photometric observations of SN2016aps in the g-, r- and i-bands were obtained using KeplerCam on the 1.2 m telescope at FLWO, MMTCam on the 6.5 m MMT telescope, the GMOS on the 8 m Gemini North telescope, and the DEep Imaging Multi-Object Spectrograph (DEIMOS) on the 10 m Keck II telescope. Images were reduced using PYRAF to apply bias subtraction and flat-fielding. Dark correction was also performed for the MMTCam images. Photometry was measured with a custom wrapper for DAOPHOT, using nearby stars from the Pan-STARRS Data Release[43] 1 to determine the point-spread function and photometric zeropoint of each image. At later epochs, FLWO images from neighbouring nights were co-added to improve the signal-to-noise ratio.

We subtracted the underlying host galaxy flux from each measurement using the galaxy magnitudes measured in late-time imaging. In the g-band, where no host imaging is available, we assumed $g_{host} \approx 24.5$ mag by interpolating across the u-, r- and i-bands. We assume a 20% uncertainty on the host flux in all cases. The change in magnitude following host subtraction becomes significant (>0.1 mag) only after ~400 d of the light curve fading, and therefore has no effect on our estimate of the total luminosity from SN2016aps.

Publicly available Pan-STARRS data in the i- and z-bands, obtained as part of the Pan-STARRS Survey for Transients[9], were downloaded from the Pan-STARRS Transient Science Server hosted at Queen's University Belfast. These magnitudes are measured by the Pan-STARRS Data Processing System[44] after subtraction of a reference image, and hence are free of host galaxy light.

Additional optical photometry was obtained by the Palomar Transient Factory (PTF) with the CFH12K camera[45] on the Palomar Observatory 48 inch telescope[46] (P48). Images were processed by the Image Processing and Analysis Center (IPAC) Image Subtraction Pipeline, which subtracts background galaxy light using deep pre-SN images and performs forced point-spread function photometry at the location of the SN[47]. The photometry is then calibrated to the PTF photometric catalogue[48]. We estimate the time of maximum light as modified Julian date (MJD) 57,404 (17 January 2016 UT) using a fourth-order polynomial fit to the PTF g-band data.

We also carried out imaging using the Neil Gehrels Swift Observatory with the UV-Optical Telescope (UVOT) in the UVW2, UVM2, UVW1, U, B and V filters. We extracted the SN flux in each image using a 3″ aperture and following the recommended procedures[49], and calibrated to Vega magnitudes in the UVOT photometric system[50]. As UV imaging covers only the first ~100 d, we assume the host contribution to be negligible in these observations.

When analysing the light curves, we accounted for a galactic extinction $E(B-V) = 0.0263$ (ref. [39]), but assumed internal extinction within the host galaxy was negligible. The galaxy appears to be a dwarf galaxy similar to the hosts of SLSNe I, which generally have low extinction (consistent with zero in many cases)[51]. At early times, the Balmer decrement (Hα/Hβ) in the spectra of SN2016aps is consistent with the expected value for case B recombination, which lends support to a low internal extinction. Finally, we do not see a strong Na I absorption line (thought to be correlated with dust extinction)[52] from the host galaxy. Including a substantial host extinction would serve to increase the total luminosity of SN2016aps even further, so would only strengthen the results presented here.

To obtain the absolute r-band and u-band light curves in Fig. 3, we used the S3 package[53] to derive cross K-corrections from our spectra. We linearly interpolated these corrections to epochs with photometry. At this redshift, observed i-band was closest to rest-frame r, and observed g to rest-frame u. The comparison data[5,6,13,14,41,54–60] in the figure were obtained from the Open Supernova Catalog[61] if possible, or otherwise directly from these papers.

The bolometric light curve was calculated using SUPERBOL[62] (v1.3), including extinction corrections, interpolation to a common set of epochs, transformation to the rest frame and blackbody fits. The bolometric light curve (on a log-linear scale), the derived temperature and radius evolution, and comparisons to other events, are shown in Extended Data Fig. 1. We assume constant colours before discovery, as we only have PTF g-band data at early times. If the photospheric temperature was higher during the rising phase, as is often the case in SNe, the total luminosity would be even greater. We also note that we do not have near-infrared data to look for dust formation, common in interacting SNe at late times[63,64]. Any late-time infrared excess, as seen[14,58,63] in the spectroscopically similar and slowly evolving SLSNe IIn SN2010jl and SN2015da, would also increase the total E_{rad} further. Thus, the integrated observed $E_{rad} = 5 \times 10^{51}$ erg is a conservative lower limit on the total energy.

To power the peak luminosity with radioactive decay would require ~ 20 $M_\odot$ of ^{56}Ni. This decays to ^{56}Co on a half-life of 6 d then to ^{56}Fe on a half-life of 77 d; thus, at peak, the energy would be primarily from ^{56}Co decays. Although we favour circumstellar interaction as the power source in SN2016aps, we note that a radioactively powered light curve still requires a huge progenitor mass consistent with a PISN: to produce 20 $M_\odot$ of ^{56}Ni needs a core mass[30] $\gtrsim 120\,M_\odot$.

X-rays. We imaged SN2016aps with the X-ray Telescope (XRT) onboard Swift. Stacking all the data for a total exposure time of 37 ks obtained between MJD 57,456.7 and 57,558.4, we detect no X-rays to a limiting count rate of $<4.2 \times 10^{-4}$ ct s^{-1}. We use the online WebPIMMS tool to convert this to flux, assuming a thermal Brehmsstrahlung spectrum with temperature $kT = 20$ keV (where k is the Boltzmann constant), similar to SN2014C[65] (one of the

best-observed interacting SNe at X-ray wavelengths), and a galactic hydrogen column density of $2.27\times10^{20}\,\mathrm{cm^{-2}}$ in the direction of SN2016aps. The unabsorbed flux is $F_X<2.0\times10^{-14}\,\mathrm{erg\,s^{-1}\,cm^{-2}}$, corresponding to a luminosity $L_X<4.7\times10^{42}\,\mathrm{erg\,s^{-1}}$ (0.3–10 keV). Taking our peak bolometric luminosity ($L_{\rm bol}$) from the UV-optical data, this implies $L_X/L_{\rm bol}<0.011$. SN2010jl had $L_X/L_{\rm bol}\approx0.01$, argued to be low due to attenuation of X-rays from the shock by the optically thick CSM[14]. Our measurement therefore implies that SN2016aps exhibits at least as much X-ray attenuation as SN2010jl.

HST imaging and host galaxy properties. We obtained late-time data using the HST on 27 July 2019 UT, corresponding to 1,017 d after maximum light in the SN rest frame (programme ID: 15709, principal investigator: M.N.). Drizzled data were downloaded from the Mikulski Archive for Space Telescopes. We used the F775W filter on the Advanced Camera for Surveys (ACS) and the F390W filter on Wide Field Camera 3 (WFC3). We matched the F390W image and an earlier image from MMTCam to the F775W image using 12 common sources. The uncertainty in the astrometric tie is 0.0282″ between the ground- and space-based images, and 0.0061″ between the two HST images. We determine the SN position to be 10 h 19 m 02.124 s, +74° 42′ 24.82″ in the system of the F775W image, using SEXTRACTOR (v2.19), with an uncertainty of 0.0084″.

The host galaxy, previously undetected in ground-based surveys, is easily identified in the HST images. We measure integrated host galaxy AB magnitudes of $m_{\rm F775W}=23.7\pm0.09$ mag and $m_{\rm F390W}=24.9\pm0.07$ mag, where we have checked using Pan-STARRS Data Release 1 sources that any deviations of the HST imaging zeropoints are smaller than the photometric errors.

An unresolved source at the same position in Keck images obtained on 26 February 2019 has an i-band measurement consistent with the ACS magnitude. We therefore assume that this measurement is host-dominated. An r-band image on the same night gives $m_{\rm r}=23.9\pm0.3$ mag.

We used GALFIT[66] (v2.0) to measure the physical size of the galaxy, finding an effective radius of $R_{\rm e}=2.1$ kpc with an axis ratio $b/a=0.27$ in the F775W image. We also find that SN2016aps is offset from the centre, as measured in red/optical light, by 3.1 HST pixels, or 0.15″. This is greater than the uncertainty in the astrometric tie between the SN and host images. Thus SN2016aps is inconsistent at the ~5σ level with having occurred in the nucleus of its host galaxy.

The F775W filter is very close to rest-frame r-band at this redshift. For an inferred absolute magnitude $M_{\rm r}\simeq-17$ mag, we estimate the galaxy stellar mass as $M_*/M_\odot\approx L/L_\odot$, where $L=10^{0.4(M_{\odot,{\rm r}}-M_{\rm r})}$, giving $M_*\approx10^{8.6}\,M_\odot$. Using the mass–metallicity relation from[67], this implies a metallicity $Z\approx0.4\,Z_\odot$. A more accurate determination of the host galaxy properties will require deep spectroscopy and imaging over a broad wavelength range after we are more confident that SN2016aps has completely faded.

The UV luminosity and spatial extent of the host indicate a mean star-formation rate surface density of ~$0.04\,M_\odot\,\mathrm{yr^{-1}}$ (ref. [68]), consistent with the lower end of the distribution measured for type I (hydrogen poor) SLSNe[69]. Those explosions are known to favour the brightest UV (most star-forming) regions of their hosts, suggesting young, massive progenitors[69]. The association of SN2016aps with the UV-brightest region of its host thus points to a massive star progenitor.

Rate estimates for interacting (P)PISNe. For each of our suggested progenitor channels, we estimate the rates of forming core masses in the necessary range via binary mergers using a pre-established method[26]. The rate is given by:

$$R=f_{\rm bin}\times f_1\times f_2\times f_{\rm sep} \quad (1)$$

where $f_{\rm bin}\simeq0.7$ is the fraction of massive stars in close binaries[70]. The next factor f_1 is the fraction of primary stars sufficiently massive to form the desired core mass post-merger (modelled using Modules for Experiments in Stellar Astrophysics[71,72]), normalized to the core-collapse SN (CCSN) rate assuming a Salpeter initial mass function and that stars with masses in the range $8-40\,M_\odot$ experience CCSNe. The factor $f_2\approx0.15$ is the fraction of secondary stars, given a suitable primary, that are sufficiently massive for this channel[26], and $f_{\rm sep}$ is the fraction of suitable binaries with the appropriate separation to merge during a given evolutionary phase. The largest uncertainty is on f_2, which can be lower by an order of magnitude for more pessimistic assumptions requiring near-equal-mass binaries[26].

For the PPISN channel, we look for existing models[24] that begin pulsing between roughly a few ×0.1–10 yr before core collapse. This corresponds to a range in helium core mass of ~$40-50\,M_\odot$. In this case, we find (from the Modules for Experiments in Stellar Astrophysics models) $f_1=0.03$. We assume the merger can happen at any point after core hydrogen burning; for a log-flat distribution of separations and a maximum stellar radius of ~$760\,R_\odot$, this gives $f_{\rm sep}=0.44$. Thus, the overall rate of formation of suitable progenitors is $R_{\rm PPISN}=0.7\times0.03\times0.15\times0.44=1.3\times10^{-3}$ per CCSN. The rate of SN2016aps-like transients will include another factor accounting for those progenitors with sufficiently rapid core rotation to form magnetars. We estimate $f_{\rm mag}\approx0.1$, that is, the fastest 10% of rapidly rotating massive stars can produce magnetars[73–75], giving an overall rate $R_{\rm PPI+mag}\approx10^{-4}$ per CCSN.

For the more massive PISN channel, the core mass range of interest[30] is ~$64-84\,M_\odot$, which gives $f_1=0.02$. However, in this case, it is less clear whether the massive merger product can retain its hydrogen envelope unless the merger happens late (after core helium burning), giving a much narrower range of allowed separations ($f_{\rm sep}\approx0.01$). In this case, the estimated rate is $R_{\rm PISN+CSM}=2.1\times10^{-5}$ per CCSN. Thus, the PPISN channel appears the more likely, even with its requirement for a central engine.

Detectability with LSST and JWST. We use our light-curve model (see also Supplementary Information) to estimate the observability of a transient like SN2016aps for next-generation instruments. MOSFIT provides a simple built-in routine to estimate the signal-to-noise for a transient observation given a specified filter and limiting magnitude. We generate synthetic light curves in the g-, r-, i- and z-bands taking the limiting magnitudes appropriate for the LSST[76]: $g_{\rm lim}=24.8$ mag, $r_{\rm lim}=24.5$ mag, $i_{\rm lim}=23.9$ mag and $z_{\rm lim}=23.3$ mag. Observations in the u- and y-bands are shallower so we do not consider them here. We place the best-fitting CSM shell model at redshifts $z=0.1$, 0.5, 0.75, 1.0, 1.5 for these simulations.

We perform the same calculation for a massive radioactively powered PISN model, based on a $130\,M_\odot$ helium core. Our MOSFIT implementation uses an ejecta mass of $130\,M_\odot$, a radioactive nickel mass of $39\,M_\odot$ and an ejecta velocity of $8{,}000\,\mathrm{km\,s^{-1}}$. Absorption by heavy elements is implemented via a linear cut-off[75] in the blackbody spectral energy distribution below 5,000 Å, to mimic the red spectra from more detailed simulations[30,77,78].

The results are shown in Extended Data Fig. 4. While both models are detectable at low redshift for 2–3 yr in the LSST survey, the situation is very different at higher redshift. Radioactive PISNe are only detected at $z\lesssim0.75$, as above this the bulk of their emission is redshifted out of the optical bands. However, a SN2016aps-like massive interacting event can be detected as far as $z\approx2$, as they do not suffer from the same rest-frame UV absorption (the power source is not coupled to heavy element production). Thus, strong CSM can increase the volume over which PISNe are detectable by up to a factor of about seven, increasing our chances of finding PISNe with LSST. However, the distribution of CSM and ejecta properties is currently unknown, and the volumetric rate of PISNe is highly uncertain (but constrained[32,79] to be $<10-100\,\mathrm{Gpc^{-3}\,yr^{-1}}$), making a quantitative estimate of the number of interacting PISNe unfeasible at this time.

We note that characteristics of a SN2016aps-like event at $z=2$ are consistent with the transient SN2213-1745, discovered[32] in stacked Canada–France–Hawaii Telescope Legacy Survey data and confirmed to be in a galaxy at $z=2.05$. This event is one of the best candidates for a PISN due to its luminosity and slow light-curve evolution, but it was found[32] that the observed flux was brighter and bluer than massive ^{56}Ni decay-powered PISN models[30]. Interaction with a massive CSM can explain this blue flux excess, while the required mass is probably still consistent with a PISN. The peak apparent magnitude $r\approx24$ confirms that events like SN2213-1745 and SN2016aps will be detectable at $z\approx2$ with LSST.

We also calculate the observability of a SN2016aps-like transient with JWST. At $z=5$, SN2016aps would have reached ~24 mag in the NIRCam F410M filter (40,900 Å in the observer frame, corresponding to ~6,800 Å in the rest frame). This matches the limiting magnitude for spectroscopy with NIRSpec to achieve a signal-to-noise ratio of 10 with the G495M disperser (covering ~30,000–50,000 Å). Thus, we could comfortably detect the strong Hα emission and spectroscopically classify a SN2016aps-like event with high confidence as far as $z\gtrsim5$.

Data availability

All data are publicly available via the Open Supernova Catalog[61] (https://sne.space) and the Weizmann Interactive SN Repository[80] (https://wiserep.weizmann.ac.il).

Code availability

MOSFiT is publicly available at https://github.com/guillochon/MOSFiT. SuperBol is publicly available at https://github.com/mnicholl/superbol.

Received: 31 January 2020; Accepted: 5 March 2020;
Published online: 13 April 2020

References

1. Schlegel, E. M. A new subclass of type II supernovae? *Mon. Not. R. Astron. Soc.* **244**, 269–271 (1990).
2. Smith, N. et al. SN 2006gy: discovery of the most luminous supernova ever recorded, powered by the death of an extremely massive star like η Carinae. *Astrophys. J.* **666**, 1116 (2007).
3. Drake, A. et al. Discovery of the extremely energetic supernova 2008fz. *Astrophys. J.* **718**, L127 (2010).
4. Chatzopoulos, E. et al. SN 2008am: a super-luminous type IIn supernova. *Astrophys. J.* **729**, 143 (2011).
5. Rest, A. et al. Pushing the boundaries of conventional core-collapse supernovae: the extremely energetic supernova SN 2003ma. *Astrophys. J.* **729**, 88 (2011).
6. Benetti, S. et al. The supernova CSS121015:004244+132827: a clue for understanding superluminous supernovae. *Mon. Not. R. Astron. Soc.* **441**, 289–303 (2014).

7. Blanchard, P. K. et al. PS16dtm: a tidal disruption event in a narrow-line Seyfert 1 galaxy. *Astrophys. J.* **843**, 106 (2017).
8. Kankare, E. et al. A population of highly energetic transient events in the centres of active galaxies. *Nat. Astron.* **1**, 865–871 (2017).
9. Huber, M. et al. The Pan-STARRS Survey for Transients (PSST)—first announcement and public release. *The Astronomer's Telegram* 7153 (2015).
10. Chornock, R. et al. Spectroscopic classification of two superluminous supernovae. *The Astronomer's Telegram* 8790 (2016).
11. Law, N. M. et al. The Palomar Transient Factory: system overview, performance, and first results. *Publ. Astron. Soc. Pac.* **121**, 1395 (2009).
12. Dong, S. et al. ASASSN-15lh: a highly super-luminous supernova. *Science* **351**, 257–260 (2016).
13. Smith, N. et al. SN 2006tf: precursor eruptions and the optically thick regime of extremely luminous type IIn supernovae. *Astrophys. J.* **686**, 467 (2008).
14. Fransson, C. et al. High-density circumstellar interaction in the luminous type IIn SN 2010jl: the first 1100 days. *Astrophys. J.* **797**, 118 (2014).
15. Sukhbold, T. & Woosley, S. E. The most luminous supernovae. *Astrophys. J.* **820**, L38 (2016).
16. Chevalier, R. A. & Irwin, C. M. Shock breakout in dense mass loss: luminous supernovae. *Astrophys. J.* **729**, L6 (2011).
17. Chugai, N. N. & Danziger, I. J. SN 1988Z: low-mass ejecta colliding with the clumpy wind? *Mon. Not. R. Astron. Soc.* **268**, 173–180 (1994).
18. Chevalier, R. A. & Irwin, C. M. X-rays from supernova shocks in dense mass loss. *Astrophys. J.* **747**, L17 (2012).
19. Mackey, J. et al. Interacting supernovae from photoionization-confined shells around red supergiant stars. *Nature* **512**, 282–285 (2014).
20. Vink, J. S. Fast and slow winds from supergiants and luminous blue variables. *Astron. Astrophys.* **619**, A54 (2018).
21. Chatzopoulos, E., Wheeler, J. C. & Vinko, J. Generalized semi-analytical models of supernova light curves. *Astrophys. J.* **746**, 121 (2012).
22. Guillochon, J. et al. MOSFiT: modular open source fitter for transients. *Astrophys. J. Suppl.* **236**, 6 (2018).
23. Dessart, L., Audit, E. & Hillier, D. J. Numerical simulations of superluminous supernovae of type IIn. *Mon. Not. R. Astron. Soc.* **449**, 4304–4325 (2015).
24. Woosley, S. E. Pulsational pair-instability supernovae. *Astrophys. J.* **836**, 244 (2017).
25. Gomez, S. et al. SN 2016iet: the pulsational or pair instability explosion of a low-metallicity massive CO core embedded in a dense hydrogen-poor circumstellar medium. *Astrophys. J.* **881**, 87 (2019).
26. Vigna-Gómez, A., Justham, S., Mandel, I., de Mink, S. E. & Podsiadlowski, P. Massive stellar mergers as precursors of hydrogen-rich pulsational pair instability supernovae. *Astrophys. J.* **876**, L29 (2019).
27. Yan, L. et al. Hydrogen-poor superluminous supernovae with late-time Hα emission: three events from the intermediate Palomar Transient Factory. *Astrophys. J.* **848**, 6 (2017).
28. Lunnan, R. et al. A UV resonance line echo from a shell around a hydrogen-poor superluminous supernova. *Nat. Astron.* **2**, 887–895 (2018).
29. Chen, T. W. et al. SN 2017ens: the metamorphosis of a luminous broadlined type Ic supernova into an SN IIn. *Astrophys. J.* **867**, L31 (2018).
30. Kasen, D., Woosley, S. E. & Heger, A. Pair instability supernovae: light curves, spectra, and shock breakout. *Astrophys. J.* **734**, 102 (2011).
31. Chatzopoulos, E. & Wheeler, J. C. Hydrogen-poor circumstellar shells from pulsational pair-instability supernovae with rapidly rotating progenitors. *Astrophys. J.* **760**, 154 (2012).
32. Cooke, J. et al. Superluminous supernovae at redshifts of 2.05 and 3.90. *Nature* **491**, 228–231 (2012).
33. Martini, P. et al. The Ohio State Multi-object Spectrograph. *Publ. Astron. Soc. Pac.* **123**, 187 (2011).
34. Fabricant, D., Cheimets, P., Caldwell, N. & Geary, J. The FAST spectrograph for the tillinghast telescope. *Publ. Astron. Soc. Pac.* **110**, 79–85 (1998).
35. Schmidt, G. D., Weymann, R. J. & Foltz, C. B. A moderate-resolution, high-throughput CCD channel for the MMT spectrograph. *Publ. Astron. Soc. Pac.* **101**, 713 (1989).
36. Hook, I. M. et al. The Gemini-North Multi-Object Spectrograph: performance in imaging, long-slit, and multi-object spectroscopic modes. *Publ. Astron. Soc. Pac.* **116**, 425–440 (2004).
37. Oke, J. B. et al. The Keck low-resolution imaging spectrometer. *Publ. Astron. Soc. Pac.* **107**, 375 (1995).
38. Perley, D. A. Fully automated reduction of longslit spectroscopy with the low resolution imaging spectrometer at the Keck Observatory. *Publ. Astron. Soc. Pac.* **131**, 084503 (2019).
39. Schlafly, E. F. & Finkbeiner, D. P. Measuring reddening with Sloan Digital Sky Survey stellar spectra and recalibrating SFD. *Astrophys. J.* **737**, 103 (2011).
40. Planck Collaboration. et al Planck 2015 results. XIII. Cosmological parameters. *Astron. Astrophys.* **594**, A13 (2016).
41. Smith, N., Chornock, R., Silverman, J. M., Filippenko, A. V. & Foley, R. J. Spectral evolution of the extraordinary type IIn supernova 2006gy. *Astrophys. J.* **709**, 856–883 (2010).
42. Savitzky, A. & Golay, M. J. E. Smoothing and differentiation of data by simplified least squares procedures. *Anal. Chem.* **36**, 1627–1639 (1964).
43. Flewelling, H. et al. The Pan-STARRS1 Database and Data Products. Preprint at https://arxiv.org/abs/1612.05243 (2016).
44. Magnier, E.A. et al. The Pan-STARRS Data Processing System. Preprint at https://arxiv.org/abs/1612:05240 (2016).
45. Rahmer, G. et al. The 12Kx8K CCD mosaic camera for the Palomar Transient Factory. *Proc. SPIE* **7014**, 70144Y (2008).
46. Law, N. M. et al. The Palomar Transient Factory: system overview, performance, and first results. *Publ. Astron. Soc. Pac.* **121**, 1395–1408 (2009).
47. Masci, F. J. et al. The IPAC Image Subtraction and Discovery Pipeline for the intermediate Palomar Transient Factory. *Publ. Astron. Soc. Pac.* **129**, 014002 (2017).
48. Ofek, E. O. et al. The Palomar Transient Factory photometric calibration. *Publ. Astron. Soc. Pac.* **124**, 62–73 (2012).
49. Brown, P. J. et al. Ultraviolet light curves of supernovae with the Swift ultraviolet/optical telescope. *Astron. J.* **137**, 4517–4525 (2009).
50. Breeveld, A. A. et al. An updated ultraviolet calibration for the Swift/UVOT. *AIP Conf. Ser.* **1358**, 373–376 (2011).
51. Lunnan, R. et al. Hydrogen-poor superluminous supernovae and long-duration gamma-ray bursts have similar host galaxies. *Astrophys. J.* **787**, 138 (2014).
52. Poznanski, D., Prochaska, J. X. & Bloom, J. S. An empirical relation between sodium absorption and dust extinction. *Mon. Not. R. Astron. Soc.* **426**, 1465–1474 (2012).
53. Inserra, C. et al. On the nature of hydrogen-rich superluminous supernovae. *Mon. Not. R. Astron. Soc.* **475**, 1046–1072 (2018).
54. Ofek, E. et al. SN 2006gy: an extremely luminous supernova in the galaxy NGC 1260. *Astrophys. J.* **659**, L13 (2007).
55. Agnoletto, I. et al. SN 2006gy: was it really extraordinary? *Astrophys. J.* **691**, 1348 (2009).
56. Miller, A. A. et al. SN 2008iy: an unusual type IIn supernova with an enduring 400-d rise time. *Mon. Not. R. Astron. Soc.* **404**, 305–317 (2010).
57. Moriya, T. J. et al. HSC16aayt: a slowly evolving interacting transient rising for more than 100 days. *Astrophys. J.* **882**, 70 (2019).
58. Tartaglia, L. et al. The long-lived type IIn SN 2015da: infrared echoes and strong interaction within an extended massive shell. *Astron. Astrophys.* **635**, A39 (2019).
59. Arcavi, I. et al. Energetic eruptions leading to a peculiar hydrogen-rich explosion of a massive star. *Nature* **551**, 210–213 (2017).
60. Terreran, G. et al. Hydrogen-rich supernovae beyond the neutrino-driven core-collapse paradigm. *Nat. Astron.* **1**, 713–720 (2017).
61. Guillochon, J., Parrent, J., Kelley, L. Z. & Margutti, R. An open catalog for supernova data. *Astrophys. J.* **835**, 64 (2017).
62. Nicholl, M. SuperBol: A user-friendly Python routine for bolometric light curves. *Res. Notes Am. Astron. Soc.* **2**, 230 (2018).
63. Gall, C. et al. Rapid formation of large dust grains in the luminous supernova 2010jl. *Nature* **511**, 326–329 (2014).
64. Bhirombhakdi, K. et al. The type II superluminous SN 2008es at late times: near-infrared excess and circumstellar interaction. *Mon. Not. R. Astron. Soc.* **488**, 3783–3793 (2019).
65. Margutti, R. et al. Ejection of the massive hydrogen-rich envelope timed with the collapse of the stripped SN 2014C. *Astrophys. J.* **835**, 140 (2017).
66. Peng, C. Y., Ho, L. C., Impey, C. D. & Rix, H.-W. Detailed structural decomposition of galaxy images. *Astron. J.* **124**, 266–293 (2002).
67. Andrews, B. H. & Martini, P. The mass–metallicity relation with the direct method on stacked spectra of SDSS galaxies. *Astrophys. J.* **765**, 140 (2013).
68. Kennicutt, J. & Robert, C. Star formation in galaxies along the Hubble sequence. *Annu. Rev. Astron. Astrophys.* **36**, 189–232 (1998).
69. Lunnan, R. et al. Zooming in on the progenitors of superluminous supernovae with the HST. *Astrophys. J.* **804**, 90 (2015).
70. Sana, H. et al. Binary interaction dominates the evolution of massive stars. *Science* **337**, 444 (2012).
71. Paxton, B. et al. Modules for experiments in stellar astrophysics (MESA). *Astrophys. J. Suppl.* **192**, 3 (2011).
72. Paxton, B. et al. Modules for experiments in stellar astrophysics (MESA): convective boundaries, element diffusion, and massive star explosions. *Astrophys. J. Suppl.* **234**, 34 (2018).
73. Yoon, S. C., Langer, N. & Norman, C. Single star progenitors of long gamma-ray bursts. I. Model grids and redshift dependent GRB rate. *Astron. Astrophys.* **460**, 199–208 (2006).
74. de Mink, S. E., Langer, N., Izzard, R. G., Sana, H. & de Koter, A. The rotation rates of massive stars: the role of binary interaction through tides, mass transfer, and mergers. *Astrophys. J.* **764**, 166 (2013).
75. Nicholl, M., Guillochon, J. & Berger, E. The magnetar model for type I superluminous supernovae. I. Bayesian analysis of the full multicolor light-curve sample with MOSFiT. *Astrophys. J.* **850**, 55 (2017).
76. LSST Science Collaboration et al. LSST science book, version 2.0. Preprint at https://arxiv.org/abs/0912.0201 (2009).

77. Dessart, L., Hillier, D. J., Waldman, R., Livne, E. & Blondin, S. Superluminous supernovae: ^{56}Ni power versus magnetar radiation. *Mon. Not. R. Astron. Soc.* **426**, L76–L80 (2012).
78. Jerkstrand, A., Smartt, S. J. & Heger, A. Nebular spectra of pair-instability supernovae. *Mon. Not. R. Astron. Soc.* **455**, 3207–3229 (2016).
79. Nicholl, M. et al. Slowly fading super-luminous supernovae that are not pair-instability explosions. *Nature* **502**, 346–349 (2013).
80. Yaron, O. & Gal-Yam, A. WISeREP—an interactive supernova data repository. *Publ. Astron. Soc. Pac.* **124**, 668 (2012).
81. Gal-Yam, A. et al. Supernova 2007bi as a pair-instability explosion. *Nature* **462**, 624–627 (2009).

Acknowledgements

M.N. is a Royal Astronomical Society Research Fellow. The Berger Time-Domain Group acknowledge NSF grant AST-1714498 and NASA grant NNX15AE50G. R.L. acknowledges a Marie Skłodowska-Curie Individual Fellowship within the Horizon 2020 European Union Framework (H2020-MSCA-IF-2017-794467). W.-f.F. and K.P. acknowledge support from NSF grant numbers AST-1814782 and AST-1909358. The Margutti group acknowledges NSF grant number AST 1909796, NASA grants 80NSSC19K0384 and 80NSSC19K0646. A.A.M. is supported by the LSST Corporation, the Brinson Foundation, the Moore Foundation via the LSSTC Data Science Fellowship Program, and the CIERA Fellowship Program. A.V.-G. acknowledges support by the Danish National Research Foundation (DNRF132). Data were obtained via the NASA/ESA Hubble Space Telescope archive at the Space Telescope Science Institute, the Swift archive, the Smithsonian Astrophysical Observatory OIR Data Center, the MMT Observatory, the MDM Observatory, the Gemini Observatory, operated by the Association of Universities for Research in Astronomy, Inc., under agreement with the NSF, and the W.M. Keck Observatory, operated as a partnership among the California Institute of Technology, the University of California, and NASA. Operation of the Pan-STARRS1 telescope is supported by NASA under Grants NNX12AR65G and NNX14AM74G. The authors respect the very significant cultural role of Mauna Kea within the indigenous Hawaiian community.

Author contributions

M.N. wrote the manuscript, led the analysis and obtained the HST and Gemini data. P.K.B. devised the selection algorithm and identified SN2016aps as an interesting source, and analysed the HST images. E.B. advised on the manuscript and leads the overall project. R.C. and K.B. obtained the MDM spectrum and classified SN2016aps. R.M. analysed the UVOT data. P.K.B., S.G., A.B. and P.C. obtained FLWO data. R.L. obtained the Keck spectra. A.V.-G. did the rate calculations. A.A.M., F.J.M. and R.R.L. provided PTF data. W.-f.F. and P.K.B. obtained MMT imaging. G.T., A.A.M. and K.P. obtained Keck imaging. All authors helped with the interpretation.

Competing interests

The authors declare no competing interests.

Additional information

Extended data is available for this paper at https://doi.org/10.1038/s41550-020-1066-7.

Supplementary information is available for this paper at https://doi.org/10.1038/s41550-020-1066-7.

Correspondence and requests for materials should be addressed to M.N.

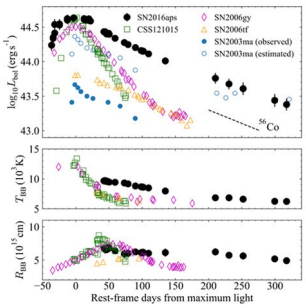

Extended Data Fig. 1 | Bolometric light curve of SN2016aps. Top: Comparison of the bolometric light curve to other SLSNe IIn. The integrated luminosity is greater than any previously known SN. Middle: Temperature evolution from blackbody fits (Methods). Bottom: Photospheric radius from blackbody fits. Error bars show 1σ uncertainties.

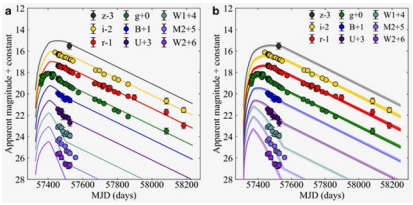

Extended Data Fig. 2 | Fit to the light curve of SN2016aps with MOSFIT using a wind-like density profile. (a) For fixed parameters based on simple scaling relations (see Supplementary Information). The fit is reasonable overall but systematically under-predicts the UV bands. (b) Realizations of a full MCMC fit. This matches the UV but favours masses larger by a factor ~ 3. Posteriors of the model parameters are given in Extended Data Fig. 3. Error bars show 1σ uncertainties.

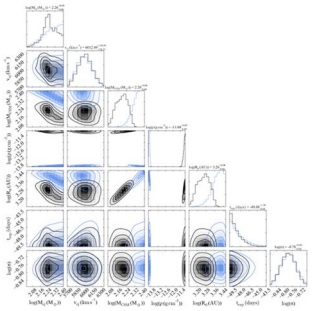

Extended Data Fig. 3 | Posteriors for physical parameters inferred using the MOSFIT CSM model. Parameters are shown for fits using both shell (ρ=constant; black) and wind ($\rho \propto r^{-2}$; blue) density profiles. The additional variance (noise) parameter, σ ~ 0.1, indicates a similar quality of fit independent of the assumed density. Both models favour ejected masses $\gtrsim 100 M_{\odot}$, with a comparable mass of CSM. Drawing from the joint M_{ej}-v_{ej} posteriors gives a kinetic energy $E_k \approx 5 \times 10^{52}$ erg in both cases.

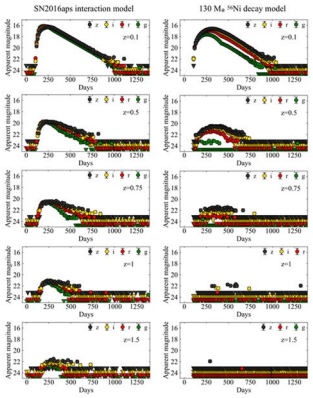

Extended Data Fig. 4 | Simulated observer frame LSST light curves in *g,r,i,z* bands. The left column shows our interaction model for SN2016aps, while the right column shows a radioactively-powered PISN model for a 130 $M_{\odot}$ helium core (Methods). The rows show the same models at redshifts z=0.1, 0.5, 0.75, 1 and 1.5. The interacting model is still well detected at z=1.5, because it is bright in the UV (whereas the radioactive model is heavily absorbed by metal lines). Therefore interacting events like SN2016aps are detectable over a volume that is larger by a factor $\gtrsim 7$. Error bars show simulated 1σ uncertainties.

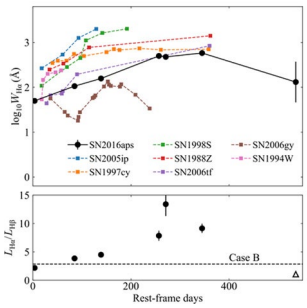

Extended Data Fig. 5 | Measurements of the Balmer lines. The equivalent width of Hα increases over the first 300 days as the continuum fades, similar to other Type IIn SNe and SLSNe, before decreasing in the final epoch. The Hα/Hβ ratio is initially consistent with recombination (horizontal line), but at later times increases to >10, indicating collisional excitation. No Hβ could be measured in the final spectrum, the arrow indicates a lower limit on this ratio. Error bars show 1σ uncertainties.

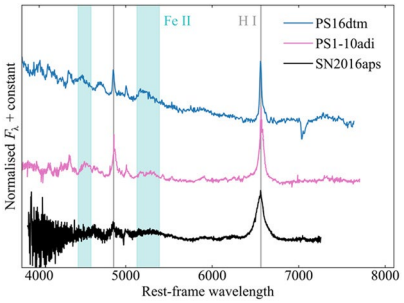

Extended Data Fig. 6 | Spectroscopic comparison of SN2016aps to the energetic nuclear transients PS16dtm and PS1-10adi. PS16dtm is thought to be a TDE [7] and PS1-10adi has been suggested to be a possible SN close to an AGN [8], these two nuclear transients closely resemble each other. The spectra shown here are at around 200 days after maximum light. SN2016aps is distinguished from these events by broader and more symmetrical Balmer lines (lacking a red shoulder), and a lack of strong, narrow Fe II emission. SN2016aps also lacks the [O III] emission seen at 5000$\AA$ (see also Supplementary Information). The apparent absorption in PS16dtm at 7000$\AA$ is a telluric feature from the Earth's atmosphere.